Check for updates

NANO · MICRO small
www.small-journal.com

Probing the Effect of Rigidity on the Cellular Uptake of Core-Shell Nanoparticles: Stiffness Effects are Size Dependent

Pratik Gurnani, Carlos Sanchez-Cano, Helena Xandri-Monje, Junliang Zhang, Sean H. Ellacott, Edward D. H. Mansfield, Matthias Hartlieb, Robert Dallmann, and Sébastien Perrier**

Nanoparticles are well established vectors for the delivery of a wide range of biomedically relevant cargoes. Numerous studies have investigated the impact of size, shape, charge, and surface functionality of nanoparticles on mammalian cellular uptake. Rigidity has been studied to a far lesser extent, and its effects are still unclear. Here, the importance of this property, and its interplay with particle size, is systematically explored using a library of core-shell spherical PEGylated nanoparticles synthesized by RAFT emulsion polymerization. Rigidity of these particles is controlled by altering the intrinsic glass transition temperature of their constituting polymers. Three polymeric core rigidities are tested: hard, medium, and soft using two particle sizes, 50 and 100 nm diameters. Cellular uptake studies indicate that softer particles are taken up faster and threefold more than harder nanoparticles with the larger 100 nm particles. In addition, the study indicates major differences in the cellular uptake pathway, with harder particles being internalized through clathrin- and caveolae-mediated endocytosis as well as macropinocytosis, while softer particles are taken up bycaveolae- and non-receptormediated endocytosis. However, 50 nm derivatives do not show any appreciable differences in uptake efficiency, suggesting that rigidity as a parameter in the biological regime may be size dependent.

1. Introduction

Polymeric nanoparticles are a promising platform for biomedical applications such as drug delivery,[1] biomedical-imaging,[2] and diagnostics.[3,4] Depending on their design, they can achieve long circulation times,[5] stealth from the immune system[6–8] and the ability to accumulate passively in tumor tissue (enhanced permeability and retention effect),[9,10] and the interactions between nanoparticles and biological systems have been extensively examined in vitro and in vivo.[11–14] Similarly, the mechanisms by which individual physicochemical properties of polymeric nanoparticles, e.g., the size,[15,16] shape,[17,18] charge[19,20] or surface functionality[21,22] influence the degree of cellular uptake have been studied exhaustively, as this is imperative for increasing their pharmacological efficacy. In contrast, despite being a key property of nanomaterials, the effect of nanoparticle

P. Gurnani,[+++] C. Sanchez-Cano,[+][++] J. Zhang, S. H. Ellacott, E. D. H. Mansfield, M. Hartlieb, S. Perrier
Department of Chemistry
University of Warwick
Gibbet Hill Road, Coventry CV4 7AL, UK
E-mail: s.perrier@warwick.ac.uk

The ORCID identification number(s) for the author(s) of this article can be found under https://doi.org/10.1002/smll.202203070.

© 2022 The Authors. Small published by Wiley-VCH GmbH. This is an open access article under the terms of the Creative Commons Attribution License, which permits use, distribution and reproduction in any medium, provided the original work is properly cited.

[+]Present address: Donostia International Physics Center, Paseo Manuel de Lardizabal 4, Donostia 20018, Spain
[++]Present address: Ikerbasque, Basque Foundation for Science, Bilbao 48011, Spain
[+++]Present address: Boots Science Building, University Park, University of Nottingham, Nottingham NG7 2RD, UK

DOI: 10.1002/smll.202203070

H. Xandri-Monje, R. Dallmann, S. Perrier
Warwick Medical School
University of Warwick
Gibbet Hill Road, Coventry CV4 7AL, UK
E-mail: r.dallmann@warwick.ac.uk

R. Dallmann, S. Perrier
Cancer Research Centre
University of Warwick
Gibbet Hill Road, Coventry CV4 7AL, UK

S. Perrier
Faculty of Pharmacy and Pharmaceutical Sciences
Monash University
381 Royal Parade, Parkville, VIC 3052, Australia

rigidity/elasticity on their behavior once inside biological systems is not fully understood.[23,24] Nanoparticle rigidity is defined in this context as the ability for nanoparticles to alter their shape in physiological conditions, and contrasts between 'hard' nanoparticles, which keep their spherical shape, and 'soft' nanoparticles, which can alter their shape from sphere to ellipsoid, etc. This gap in knowledge on particle physical attributes is even more surprising considering how important the mechanical properties of materials are for maintaining particular biological functions.[25–27]

Currently, several studies indicate the fast and effective phagocytosis of rigid nanomaterials by macrophages when compared with their softer analogs.[23,28,29] This can help to explain the longer blood circulation times and increased tumor accumulations normally observed for softer nanoparticles.[24,29–31] On the contrary, it is not clear if soft[23,32,33] or hard[34,35] nanomaterials would penetrate better inside tumors. Furthermore, there is no consensus on whether harder[30,35–37] or softer particles[33,37–39] are preferentially internalized by cancer cells. So far, investigations performed to test the effect of rigidity on cell uptake have yielded conflicting results, with either rigid or flexible particles taken up in greater quantities,[40,41] depending mostly on the type of cancer cell used for the study.[23,24] Based on simulation data, the widely accepted explanation for a difference in uptake between soft and hard nanoparticles is the ability of soft particles to deform when interacting with cellular surfaces.[42,43] On the one hand, deformation can increase the adhesion energies required for complete internalization of single particles (making internalization of hard > soft), while on the other hand also increasing the chance for co-operative uptake, i.e., combined effects caused by the simultaneous interaction between two or more particles and the cell membrane facilitates the cellular uptake of the particles, which occurs at once (making internalization soft > hard). Unfortunately, simulation data cannot paint the entire picture for nanoparticle interactions with complex biological systems.

Experimentally, however, the lack of consensus on the degree of cellular uptake of particles may arise from the range of methods used to achieve control over the rigidity of the particles. In previous reports, nanoparticle rigidity has been tuned using different methods. For example, the rigidity of colloidal hydrogels[44] can be modified by increasing or decreasing the crosslinking density,[45] which regulates the water content within the core of the particles directly impacting the flexibility of the nanoparticles, but also potentially modifying the hydrodynamic volume the particles occupy.[30] Rigidity of layer-by-layer(LbL)/templated nanocapsules[46] can be also adapted by tuning the charge density and/or number of layers of oppositely charged polyelectrolytes present on nanocapsules.[38] Hybrid lipid-nanoparticle[35] and core-shell silica systems[23] can control their rigidity by changing the precursors or the thickness of their lipidic layers (i.e., monolayer or bilayers) or shells, altering their surface properties in the process. Thus, in most of those cases, alterations of physicochemical nanoparticle properties other than rigidity (i.e., size, shape, hydrophobicity) may have a substantial effect on cellular internalization, which, so far, made it challenging to study the impact of particle rigidity in isolation.

Traditionally the flexibility of bulk materials can be controlled using the variation of the glass transition temperature (T_g) of different polymeric matrices.[47] As T_g is an intrinsic material property, this method poses significant advantages over other techniques as one simply has to choose the correct monomer composition to tune nanoparticle rigidity around physiological conditions.[48] Therefore, a polymer nanoparticle with a T_g above 37 °C should be 'hard' in physiological conditions, whereas it should be 'soft' with a T_g below 37 °C. This method has been used to modify the rigidity of nanoparticles (synthesized via miniemulsion polymerization) by increasing the alkyl side chain lengths of polymethacrylates (poly(methylmethacrylate) to poly(stearylmethacrylate)). The resulting decrease in T_g triggered an increase in cellular uptake of nanoparticles tested in a wide range of cell lines.[49] However, the use of longer side chains also led to an increased surface hydrophobicity, which is known to drastically impact cellular uptake.[21]

To isolate the individual effect of rigidity, nanoparticles with different T_g should have identical surface chemistry and changes in hydrophobicity and other physical properties have minimal impact in their internalization. For example, poly(ethyleneglycol)-b-(poly(e-caprolactone)-g-poly (butylacrylate)) particles with different rigidities were prepared by atom transfer radical polymerization (ATRP) by altering the length of the butylacrylate hydrophylic chains, and their tumor penetration properties studied both in vitro and in vivo. Yet, their cellular internalization was not studied independently.[32] Alternatively, a technique that can also achieve such properties is RAFT emulsion polymerization, which combines RAFT polymerization[50–52] and conventional emulsion polymerization[53] producing stable monodisperse core-shell nanoparticles, with the corona chemistry imparted by the hydrophilic section of an amphiphilic macro-RAFT agent stabilizer. Since its conception, RAFT emulsion polymerization has been used to generate uniform nanoparticles with various sizes,[54] shapes,[55] and surface functionalities[56,57] by simply changing the reaction parameters of the emulsion polymerization, or the monomer composition[56,58,59] of the starting macro-RAFT agent. Nanoparticles synthesized with this approach lend themselves to fundamental studies of rigidity, as such particles maintain their structural integrity at low concentration, with precise control over both the nanoparticle core and surface.[60,61]

Our aim in this work was to elucidate the effects of nanoparticle rigidity across multiple particle sizes on their biological properties, both in vitro and in vivo. We report the synthesis of a series of inert uniform PEGylated core-shell nanoparticles (with diameters of 50 and 100 nm) synthesized via RAFT emulsion polymerization with three differing core rigidities / T_g and identical surface chemistry. These are used to evaluate possible differences caused by nanoparticle rigidity on cellular uptake, intracellular trafficking, and biodistribution.

2. Results and Discussion

2.1. Nanoparticle Synthesis and Characterization

A series of 50 and 100 nm core-shell nanoparticles with the same inert polymeric shell and three different T_g cores

© 2022 The Authors. Small published by Wiley-VCH GmbH

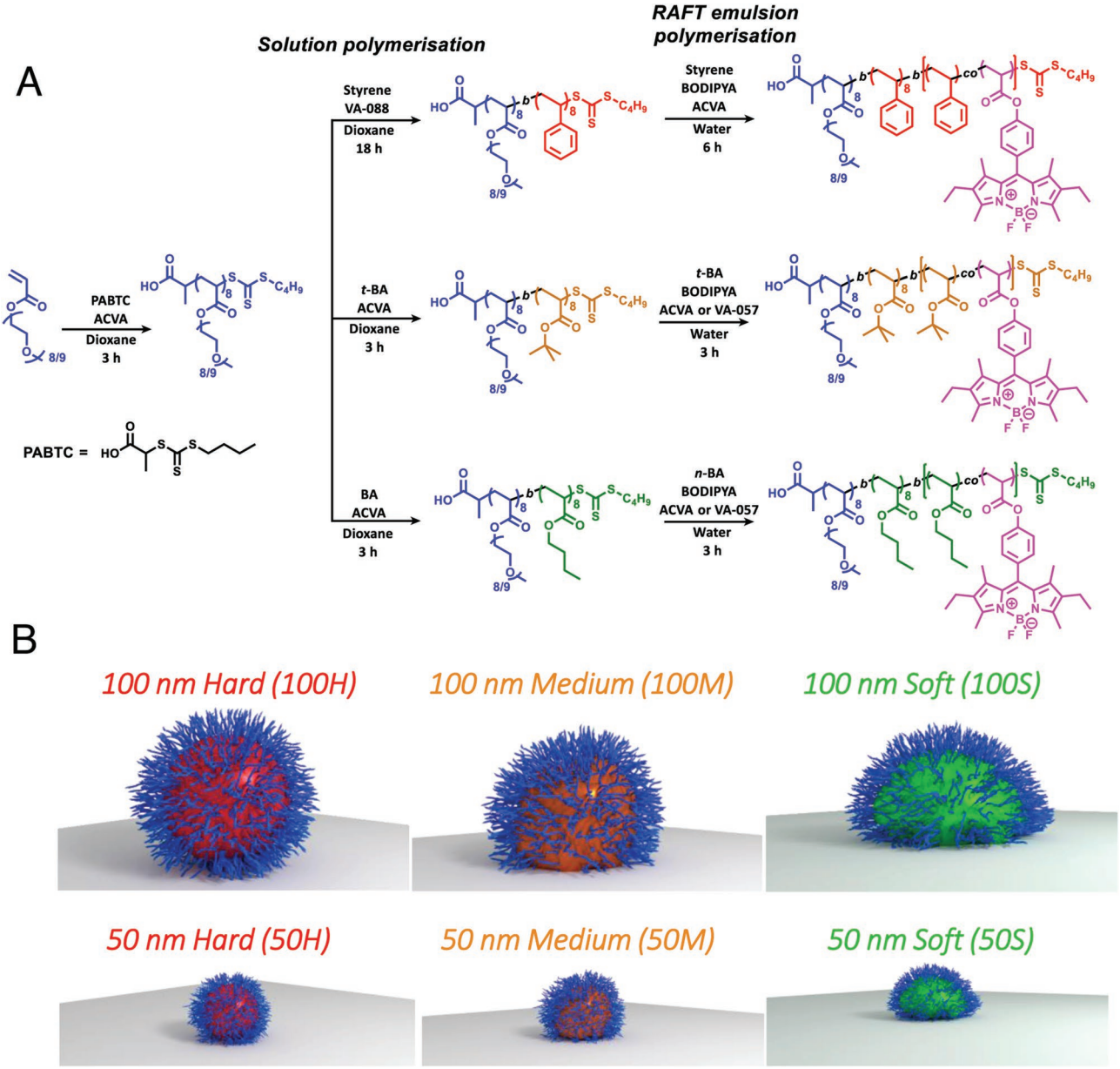

Figure 1. A) Preparation of core-shell nanoparticles via RAFT emulsion polymerization. B) Graphical representation of 100 and 50 nm hard, medium, and soft nanoparticles.

(polystyrene (PS; $T_{g,lit}$ = 100 °C),[62] poly(*tert*-butyl acrylate) (P(*t*-BA; $T_{g,lit}$ = 43 °C)[62] and poly(*n*-butyl acrylate) (P(*n*-BA); $T_{g,lit}$ = −54 °C)[62] for the hard ($50H_{NF}$ and $100H_{NF}$), medium ($50M_{NF}$ and $100M_{NF}$), and soft ($50S_{NF}$ and $100S_{NF}$) particles respectively were prepared using RAFT emulsion polymerization, and following previously reported synthetic conditions.[56,60,63,64] Briefly, amphiphilic macro-RAFT agents $P(PEGA)_8$-PS_8, $P(PEGA)_8$-$P(t\text{-}BA)_8$ and $P(PEGA)_8$-$P(n\text{-}BA)_8$ stabilizers were self-assembled in aqueous solution and chain extended in emulsion with styrene, *t*-BA and *n*-BA respectively (**Figure 1**). The particle size was controlled by modifying the monomer, initiator, and macro-RAFT agent concentrations as well as the DP_{target} during the emulsion polymerizations (Table S1, Supporting Information). This macro-RAFT agent design imparts a dense PEG brush and negative charge at the particle surface, increasing biocompatibility and solution stability. Fluorescently labeled nanoparticles were also prepared by the addition of 1% (wt/wt, with respect to the hydrophobic monomer) boron-dipyrromethene acrylate (BODIPYA) to the RAFT emulsion polymerizations (Figures S1–S3, Supporting Information). This approach is advantageous because BODIPYA only labels the core of the nanoparticle and, thus, does not alter its surface properties.

Monomer consumptions for all polymerizations were found to be >98% (measured using gravimetric technique), as expected for all emulsion polymerizations. Initial DLS analysis of the particles (both fluorescent and non-fluorescent) showed low polydispersities (PDi ≈ 0.05) at, or close to, the targeted

© 2022 The Authors. Small published by Wiley-VCH GmbH

Table 1. Characterization data of synthesized nanoparticles.

			Hydrodynamic diameter and ζ-potential					
			Water			DMEM		
Full title	Core	Abbreviation	Average diameter [nm][a)]	PDi[b)]	ζ-potential [mV][c)]	Average diameter [nm][a)]	PDi[b)]	T_g °C[−1d)]
100 nm Hard	PS	100H	107.6 ± 3.6	0.054	−31.6 ± 5.6	112.4 ± 5.4	0.051	90.0
100 nm Medium	P(*t*-BA)	100M	102.7 ± 4.2	0.056	−25.3 ± 4.2	102.8 ± 4.8	0.082	37.8
100 nm Soft	P(*n*-BA)	100S	101.5 ± 3.4	0.058	−28.4 ± 3.5	104.7 ± 6.2	0.062	−57.5
50 nm Hard	PS	50H	53.6 ± 2.1	0.062	−24.3 ± 2.1	52.7 ± 3.1	0.058	90.0
50 nm Medium	P(*t*-BA)	50M	57.9 ± 2.5	0.056	−35.9 ± 3.2	49.1 ± 2.1	0.065	31.4
50 nm Soft	P(*n*-BA)	50S	54.2 ± 2.9	0.047	−30.9 ± 6.5	55.4 ± 2.9	0.050	−58.3

[a)]Mean of three measurements using dynamic light scattering (number distribution) and standard deviation; [b)]Calculated using Equation S1 (Supporting Information); [c)]Mean of three measurements and standard deviation; [d)]Measured using differential scanning calorimetry.

diameters (**Table 1**, **Figure 2**; Table S2, Figures S4 and S5, Supporting Information). This was independently confirmed from TEM micrographs (Figure 2). A negatively charged carboxylated particle corona was confirmed with particles exhibiting zeta potentials of ≈ −30 mV (Table 1; Table S2, Supporting Information). UV-detection SEC revealed successful incorporation of the BODIPYA monomer, and good molecular weight control of the polymers comprising the nanoparticles (Figures S6 and S7, Supporting Information). However, significant amounts of BODIPYA and the macro-RAFT agent remained unconsumed (Figure S6, Supporting Information), which could leak from the particles yielding erroneous results in cellular uptake studies.[64,65] To remove the free fluorophore, particles were purified by dialysis against a 1,4-dioxane/ water mixture (60/40, v/v) to remove unconsumed BODIPYA and macro-RAFT agent (monitored by THF-SEC), followed by dialysis against pure water to eliminate residual 1,4-dioxane (Figure S6, Supporting Information). In all cases, particle size and PDi did not change after purification (Figure S4, Supporting Information). Negligible differences in hydrodynamic diameter and PDi were observed when particles were suspended in Dulbecco's modified eagle cell culture medium (DMEM; Table 1; Table S2, Supporting Information), suggesting they would be colloidally stable during cellular experiments.

Spherical morphology was confirmed using small angle neutron scattering (SANS) measurements performed on the 100 nm particles. These measurements also revealed that all three particles, regardless of core materials displayed similar polymer aggregation number (N_{agg}) per particle, suggesting a similar PEG brush density at the particle surface (Figure S8, Supporting Information). Furthermore, T_g determined using differential scanning calorimetry (DSC) confirmed that hard, medium and soft nanoparticles were generated from PS, P(*t*-BA) and P(*n*-BA) nanoparticles, respectively (Figures S9 and S10, Supporting Information). Full characterization of the fluorescent and non-fluorescent nanoparticles can be found below (Table 1) and in the supplementary information (Table S2, Supporting Information), respectively. Height profiles of each of the nanoparticles were measured using atomic force microscopy (AFM) and confirmed the expected rigidity. Hard derivatives matched the theoretical heights, while the lower T_g of the medium (T_g ≈ 37 °C) and the soft (T_g ≈ −57 °C) particles caused flattening as observed by the reduced particle heights (≈50% and 95% respectively for 100 nm particles and, 75% and >90% for 50 nm particles respectively) (Figure 2). Overall, the comprehensive analysis of the nanoparticles indicated that the only major differences between the nanoparticles were rigidity and size (between 50 and 100 nm families), with other parameters such as surface chemistry, brush density and zeta-potential being identical.

2.2. Toxicity and Membrane Activity

The biocompatibility of the synthesized particles was confirmed by determining their membrane activity and in vitro growth inhibition. Erythrocytes incubated with multiple concentrations (0.1, 0.05, and 0.01 mg mL^{-1}) of 100 and 50 nm hard, medium, and soft nanoparticles (1 h at 37 °C) all displayed very low hemolysis (<5%) compared to Triton-X (positive control), indicating low membrane interaction (Figure S11, Supporting Information). Furthermore, none of the hard, medium, or soft nanoparticles inhibited the growth in a panel of 4 human cell lines at concentrations up to 500 μg mL^{-1} after incubation for 72 h (Figure S12, Supporting Information).

2.3. In Vitro Cellular Uptake Studies

BODIPYA labeled nanoparticles were used to examine the effect of rigidity on uptake in mammalian cells. Experiments were performed with 100 and 50 nm particles at the same mass concentration (e.g., 100 μg mL^{-1}), these concentrations equate to 1.9×10^{11} particles mL^{-1} and 1.5×10^{12} particles mL^{-1}, respectively due to the difference in volumes between particles of different sizes (Equation S4, Supporting Information). For clarity, internalization was compared within the same particle size (i.e., uptake of 100 nm particles is only compared to the other 100 nm particles, not to the 50 nm analogs and vice versa). The relative cellular internalization was normalized to soft particles (100S for 100 nm particles, and 50S for 50 nm particles) by using ratios of relative emission obtained from calibration curves performed at different concentrations of each of the nanoparticles (Figure S13 and Table S3, Supporting Information).

The optimal particle concentration for uptake experiments was determined by incubating cells with different

© 2022 The Authors. Small published by Wiley-VCH GmbH

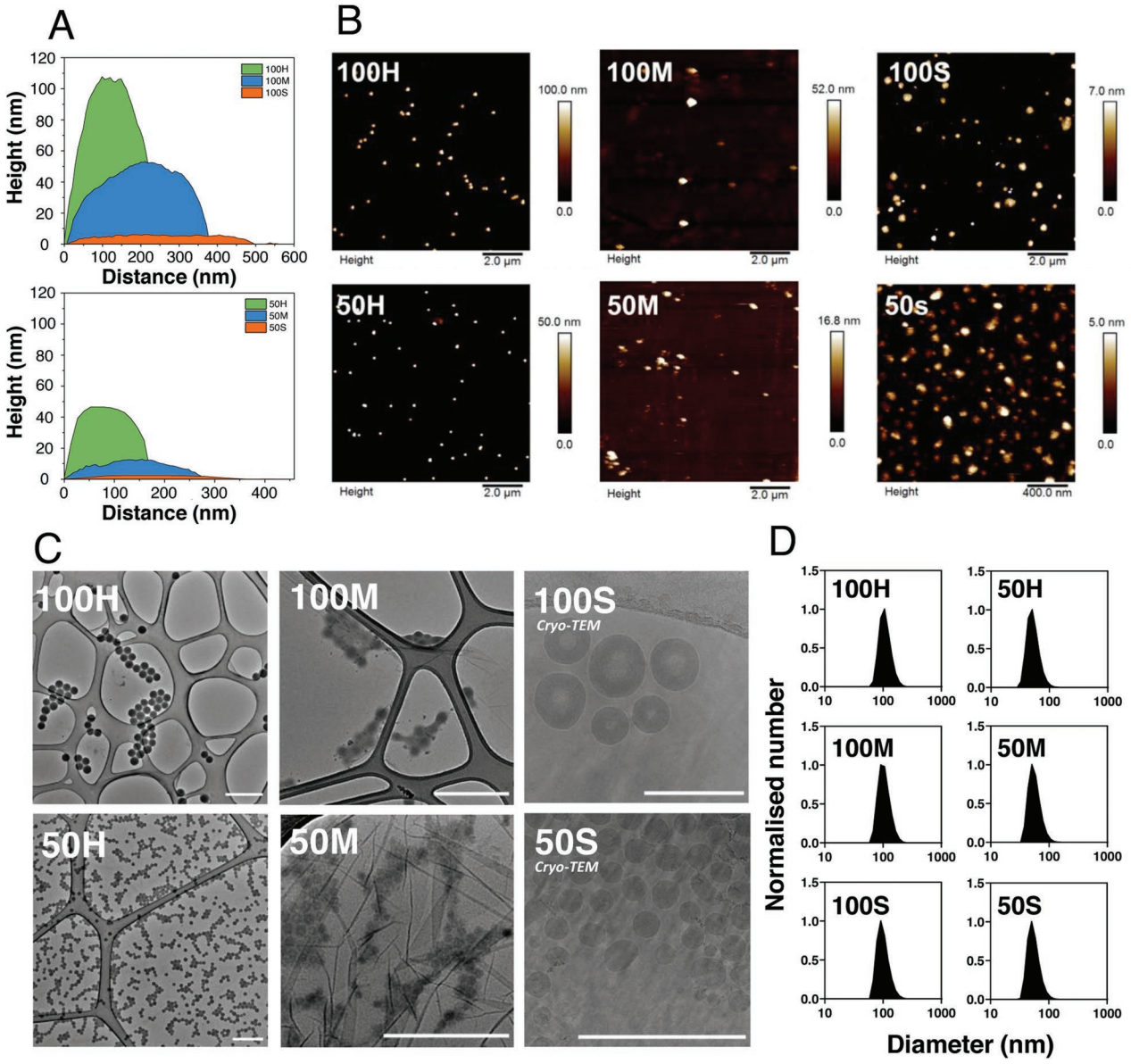

Figure 2. A) Height profiles of single 100 and 50 nm particle with hard (green), medium (blue), and soft (orange) rigidities determined by AFM. B) Representative atomic force micrographs for the 100H, 100M, 100S, 50H, 50M, and 50S nanoparticles. Calibration bars indicate the maximum height as measured by atomic force microscopy C) TEM images (100H, 100M, 50H, 50M) and Cryo-TEM images (100S and 50S) of nanoparticles, scale bars are 500 nm in length, please note all images are taken with different magnification. D) Particle size distributions in solution as measured by dynamic light scattering measured at room temperature.

concentrations (50, 100, and 200 µg mL^{-1}) of hard, medium, and soft nanoparticles for 2 h (Figure S14, Supporting Information). Intracellular fluorescence was acquired using a cell imaging plate reader, and then corrected and normalized as described. 100 µg mL^{-1} was selected, as it allowed reliable detection of BODIPYA fluorescence, while avoiding saturation and toxicity problems. These initial experiments also showed that intracellular fluorescence increased with higher doses. Furthermore, significantly higher uptake efficiency was observed for 100S compared with 100M and 100H analogs ($p < 0.01$), whilst 50 nm particles showed no clear relation between internalization and rigidity.

For our in vitro experiments we chose two model cell lines derived from a grade IV prostatic adenocarcinoma (PC3), and a colorectal adenocarcinoma (Caco-2). These were chosen based on previous studies, both in our lab and from the literature which showed high tolerability toward a range of nanoparticle systems and are capable of internalizing them through a range of endocytosis mechanisms.[66–74] Alternatively, Caco-2 cells are a common model for intestinal absorption of both drugs and nanoparticles.

PC3 and Caco-2 cells were then incubated with 100 and 50 nm nanoparticles (hard, medium, and soft), for 2, 4, and 24 h (**Figure 3**A,B). For the 100 nm particles, Figure 3 shows

© 2022 The Authors. Small published by Wiley-VCH GmbH

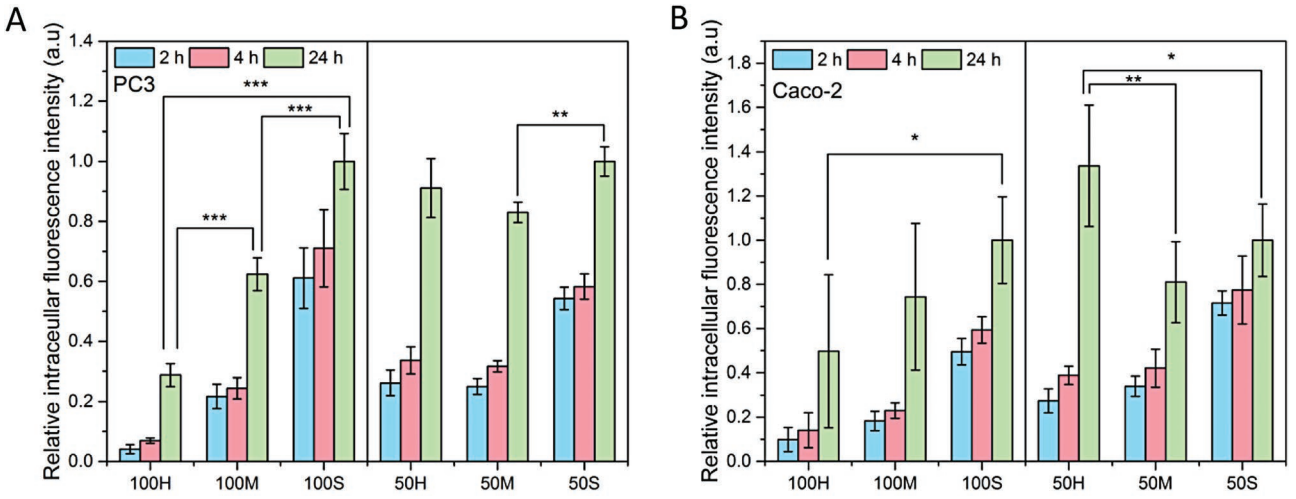

Figure 3. Relative fluorescence intensity post-incubation with nanoparticles of varying rigidity inside A) PC3 cells and B) Caco-2 at a nanoparticle concentration of 100 μg mL^{-1} as a function of incubation time (2, 4, and 24 h). Fluorescence intensities are normalized to 100S and 50S for 100 and 50 nm particles respectively. The mass concentrations equate to 1.9×10^{11} particles mL^{-1} and 1.5×10^{12} particles mL^{-1} for the 100 and 50 nm particles (Equation S4, Supporting Information). Data represents the mean ± standard deviation for two independent experiments each repeated with triplicates ($n = 3$). Asterisks indicate relevant statistically significant results (*$p \leq 0.05$, **$p \leq 0.01$, ***$p \leq 0.001$) determined from an ANOVA and post-hoc Tukey–Kramer test.

that cells treated with 100H internalized much less after 2 and 4 h than cells treated with 100S (typically by a factor 5), and 100M (typically by a factor 2). Looking at the 24 h assay, the 100S particles internalized more than the 100M and at least twice as much as the 100H. Strikingly, our experiments showed that PC3 cells treated for 24 h with 100H internalized only half the number of particles found in cells treated for 2 h with 100S. Therefore, uptake efficiency and rate for 100 nm particles were higher for soft particles. 100S particles were observed to be taken up in greater quantities and more rapidly than their medium and hard analogs. Still, we could not say if the increased quantities of soft particles observed inside cells were due to improved uptake of single particles, or to the presence of cooperative uptake paths favoring the adhesion and aggregation of soft NPs to the cellular membrane. In contrast, the number of particles internalized by cells after 24 h treatment with 50H, 50M or 50S did not vary with rigidity, although the uptake rate was still faster for soft nanoparticles when compared with that of medium and hard ones (which showed equivalents uptake rates). Nevertheless, the differences between the uptake rates of 50S and 50M/50H (2× slower or less) were always significantly smaller than those observed between the equivalent 100 nm particles (over 3× slower for medium and 6× for hard particles). Previously, Vogt and co-workers reported that for thin films with >100 nm film thickness, the elastic moduli matched those of bulk materials. However, if the thickness of the film was <50 nm, the onset of confinement effects reduced the difference in elastic moduli for materials with differing T_g, making the elastic modulus of the films more similar to each other.[75] This could explain the differences that we observe for the internalization of our particles. Rigidity should influence both degree and rate of cellular uptake if particles behaved as bulk materials (>50 nm diameter systems; soft nanoparticles are preferred over medium and hard nanoparticles). However, it is possible that at smaller sizes (below 50 nm diameter) the rigidity differences are much smaller, or even negligible, thus reducing the effect on the uptake rate and maybe other processes (such as particle efflux) involved in the overall cellular uptake.

2.4. Uptake Pathways of Core-Shell Polymeric Nanoparticles

Cellular uptake of nanoparticles is largely governed by energy-dependent processes such as phagocytosis, receptor mediated- and non-receptor mediated endocytosis.[76,77] However, the individual physicochemical properties of nanoparticles are known to influence the mechanism by which they are taken up by cells.[78,79] The energy-dependent uptake for the 100 and 50 nm particles was evaluated by performing internalization experiments at 4 °C on both PC3 and Caco-2 cells. A reduction of intracellular fluorescence by ≈60–70% ($p \leq 0.001$) was observed (**Figure 4**A; Figure S15, Supporting Information), suggesting a strong preference for an energy-dependent uptake mechanism (most likely some form of endocytosis). To further determine the relative contributions of the various well-known uptake mechanisms for each of the nanoparticles studied, clathrin-mediated endocytosis, macropinocytosis and caveolae-mediated endocytosis were each blocked by co-incubation with pharmacological inhibitors (chlorpromazine, amiloride, and genistein, respectively), and particle uptake monitored as before (Figure 4B; Figure S16, Supporting Information). Inhibition of clathrin-mediated endocytosis and macropinocytosis led to a significant decrease in the internalization of hard particles (both 100 and 50 nm showed ≈ 60% and 40% reduction, respectively, with respect to a control which was not treated with any inhibitor and is shown as a red dotted line in Figure 4B), but not medium or soft. Remarkably, 50M and 50S showed an 80% increase in accumulation after macropinocytosis was inhibited, which has previously been attributed to a reduction of

© 2022 The Authors. Small published by Wiley-VCH GmbH

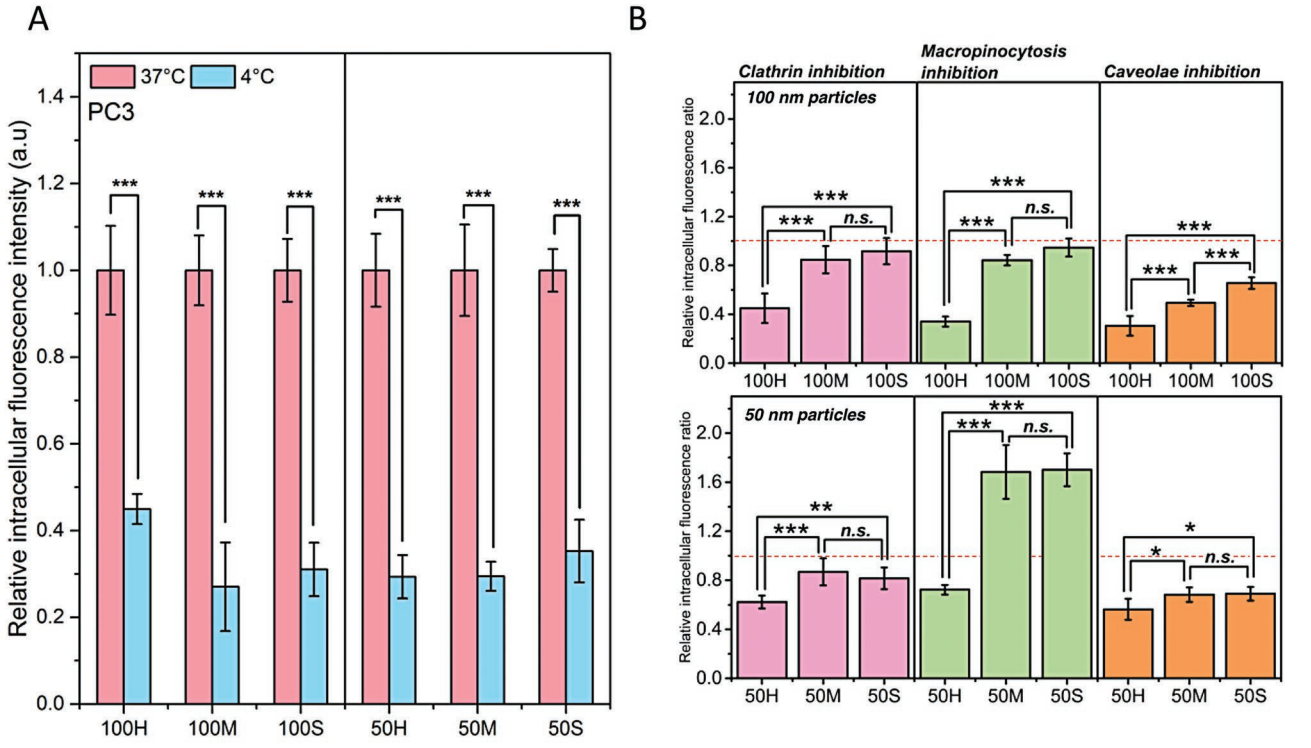

Figure 4. Relative fluorescence intensity post-incubation with nanoparticles (100 μg mL^{-1}) of varying rigidity inside A) PC3 cells for 2 h at 4 °C shutting down ATP production, normalized to a control at 37 °C to highlight the amount of uptake due to active transport B) PC3 cells for 2 h additionally pre-treated with inhibitors for clathrin- (chlorpromazine) and caveolae- (genistein) mediated endocytosis and macropinocytosis (amiloride) normalized to a control which was not treated with any inhibitor (represented as the red dotted line at 1.0). Data represent the mean ± standard deviation for two independent experiments each repeated with triplicates ($n = 3$). The mass concentrations equate to 1.9×10^{11} particles mL^{-1} and 1.5×10^{12} particles mL^{-1} for the 100 and 50 nm particles (Equation S4, Supporting Information). Asterisks indicate relevant statistically significant results (*$p \leq 0.05$, **$p \leq 0.01$, ***$p \leq 0.001$) and *n.s.* represents not significant results determined from an ANOVA and post-hoc Tukey–Kramer test.

nanoparticle exocytosis.[80] In contrast, inhibition of caveolae-mediated endocytosis led to a reduction in the accumulation of all six particles.

Our results indicate that nanoparticle rigidity significantly affects the cellular uptake mechanism, with soft and medium particles seemingly going through caveolae-mediated endocytosis or other non-specific receptor-independent mechanisms, while hard nanoparticles are transported through a combination of the three endocytosis pathways tested. Moreover, a correlation between rigidity and the extent of caveolae-related uptake was observed for 100 nm particles (70% > 55% > 30% reduction, for 100H, 100M, 100S, respectively). This dependence on caveolae-mediated endocytosis has been previously reported for large 1 μm hydrogel particles, but not on the nanoscale (below 1 μm).[39] Interestingly, caveolae are known to act as mechanosensors capable of responding to mechanical stress.[81,82] It is therefore possible that particles with increased rigidity induce a greater caveolae-mediated response upon interaction with the cell membrane. Furthermore, the negligible rigidity differences between 50 nm analogs could explain why internalization of 50H, 50M, and 50S by caveolae-mediated endocytosis was independent of their T_g (reduction of ≈40–50% for all three). This is further supported by activity studies on eukaryotic mimicking lipid 1,2-dimyristoyl-sn-glycero-3-phosphoryl-choline membranes (DMPC) via quartz crystal microbalance with dissipation monitoring experiments. These revealed a strong interaction for 100H particles in comparison to 100S, while all 50 nm derivatives showed negligible interference regardless of rigidity (Figure S17, Supporting Information).

Confocal laser scanning microscopy (CLSM) on live PC3 cells treated with the 100 nm nanoparticles showed the same trend of internalization efficiency previously described (100S > 100M > 100H) after 2, 4, and 24 h incubation, while again 50 nm particles displayed minimal differences with of core rigidity (**Figure 5**). Furthermore, a high degree of colocalization between fluorescent nanoparticles and LysoTracker (Pearson's correlation coefficient = >0.65) was observed, with all particles reaching the lysosome within 2 h of incubation (Table S6 and Figure S19, Supporting Information). Experiments performed at 4 °C confirmed that our nanoparticles were likely internalized through an energy-dependent endocytosis mechanism (Figure S18, Supporting Information). Interestingly, soft microcapsules (>1 μm diameter) have been previously described to accumulate faster in the lysosome as compared to stiff ones.[38] However, there were no obvious differences in the intracellular distribution between soft and hard nanoparticles in our experiments. Overall, this is in line with the uptake experiments, and confirmed the conventional endosomal-lysosomal trafficking route as the main internalization pathway for these nanoparticles regardless of rigidity.

© 2022 The Authors. Small published by Wiley-VCH GmbH

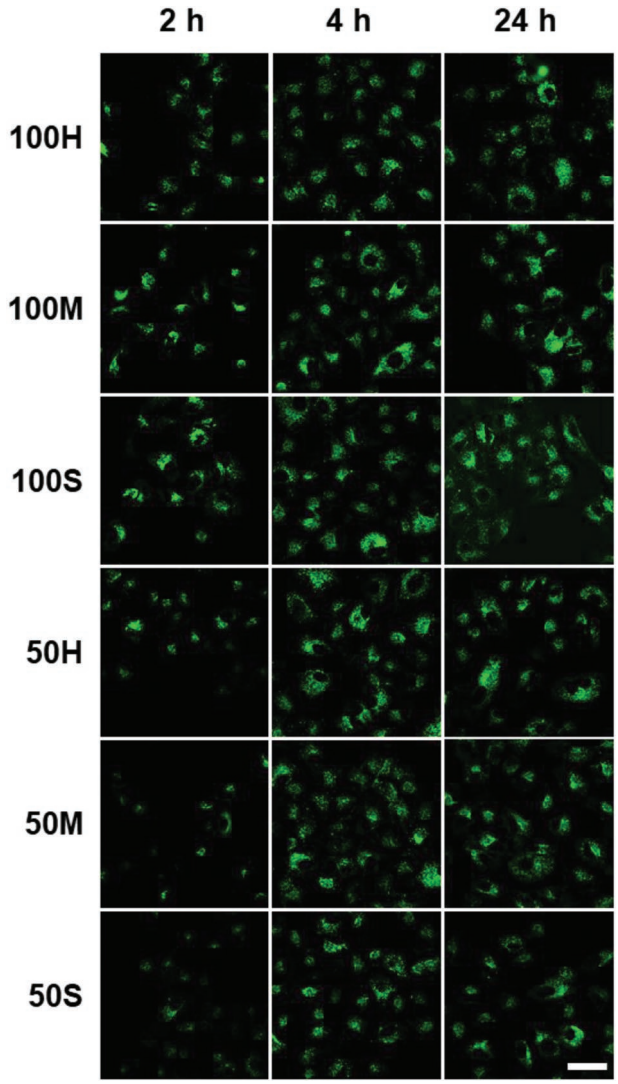

Figure 5. CLSM images of PC3 cells incubated for indicated times (2, 4, 24 h) with 100 μg mL^{-1} of 100H, 100M, 100S, 50H, 50M and 50S nanoparticles. The mass concentrations equate to 1.9×10^{11} particles mL^{-1} and 1.5×10^{12} particles mL^{-1} for the 100 and 50 nm particles (Equation S4, Supporting Information). Scale bar is 50 μm in length.

2.5. In Vivo Biodistribution Studies

Given the rigidity-dependent differences in cellular uptake for the 100 nm nanoparticles, we investigated the in vivo distribution profile of hard and soft varieties in mice. For this, subcutaneous tumor-bearing mice were injected intra-peritoneally (i.p.) with 100 μL fluorescent 100S and 100 H nanoparticles (1000 μg mL^{-1}) and the accumulation in different tissues was determined ex vivo by measuring the fluorescence intensity of blood and organ homogenates 1, 2, 4, 8, and 24 h post injection. Over the entire time course, the resulting pharmacokinetic profile for both nanoparticles was similar and followed the expected[83] increase in serum concentration over the first 8 h, as the nanoparticles enter into systemic circulation. Then, between 8–24 h, we observed a decrease in the serum concentration and an increase in splenic and hepatic accumulation. No significant differences were observed between 100H and 100S accumulation in the lungs, spleen, blood, tumor, or liver at any time point. Equally, although a moderate amount of 100H and 100S accumulated in the Hepa1-6 tumors, only minimal differences in tumor fluorescence were evident between particle rigidities. In contrast, hard and soft nanoparticles accumulated differently in the kidney (2–24 h), which may indicate that rigidity of the particles could affect renal clearance (**Figure 6**A). Furthermore, when the concentration of particles in each organ is expressed as % of total nanoparticles, it can be observed that accumulation of the harder nanoparticles in the spleen is twofold greater compared with the softer analogs (at each time point). This could indicate a preference of macrophages to phagocyte harder nanoparticles (observed previously in vitro with particles larger than 200 nm), followed by trafficking to the spleen (Figure 6C).[84]

These observations were complemented by a second non-tumor-bearing mouse cohort that was i.p. injected with the same dose of nanoparticles and then followed up for 1, 7, and 28 days. Consistent with the first in vivo experiment, the amounts of hard and soft particles found in blood, liver, and spleen were comparable. However, in lungs and kidneys, we found a two- threefold more softer particles compared with harder analogs (Figure 6B,D).

Overall, our experiments show more subtle differences in the in vivo biodistribution compared to our in vitro results with nanoparticles of different rigidities. This may be attributed to differences under flow conditions, or the formation of an equivalent protein corona around each of the particles due to their similar surface properties, which would warrant further exploration of the significance for translational project.

It is important to understand all aspects of nanoparticle distribution and excretion for their utility as drug delivery vehicles in experimental models like mice as well as guide extrapolation to patients. Physiology based pharmacokinetic (PBPK) modeling can help to understand the relationship between nanoparticle traits and their in vivo behavior and guide optimization of the particles. To this end, PKPB models describing nanoparticle behavior in vivo have been established,[85] taking into account parameters such as size, surface charge, or functionality. To date, however, these are unsuited to describe our data as no parameter has been described for rigidity of nanoparticles, and future studies should take this into account when further exploring the potential of particle rigidity.

3. Conclusion

By employing nanoparticles of two sizes varying only by the glass transition temperature of the polymers forming their core, we have been able to selectively examine and identify the role of particle rigidity for cellular uptake in vitro and for biodistribution in vivo. Our findings clearly indicate that rigidity can have a significant effect on these processes, suggesting that softer nanoparticles are internalized faster and to a greater degree than harder analogs in the cancer cell lines studied.

© 2022 The Authors. Small published by Wiley-VCH GmbH

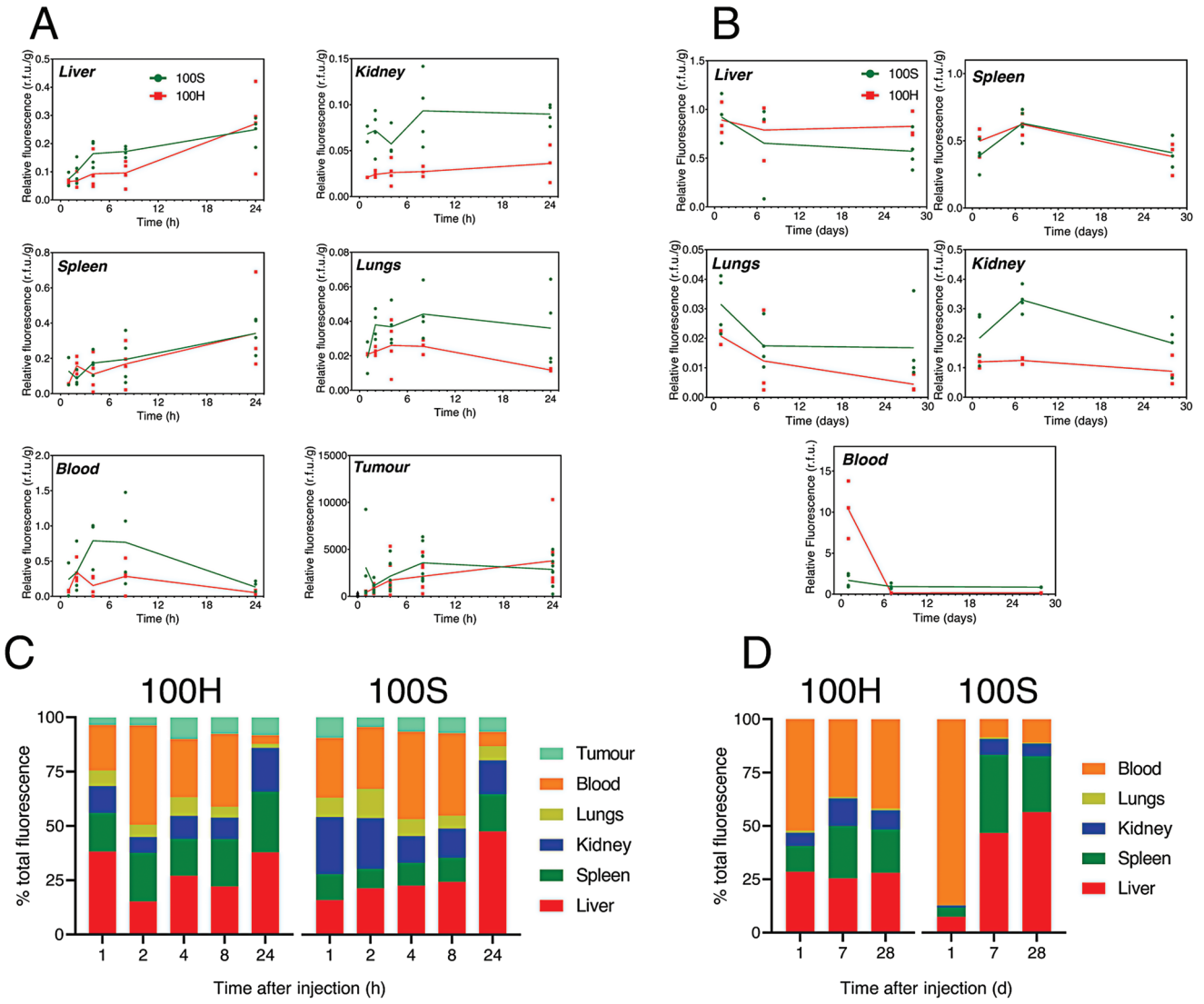

Figure 6. Relative accumulation of 100H (red) and 100S (green) nanoparticles after a single i.p. injection (100 µL at 1000 µg mL^{-1}) in the liver, kidney, spleen, lungs, blood and xenograft Hepa1-6 tumors. Organs were sampled at 1, 2, 4, 8, and 24 h for the A,C) short-term experiment, and after 1, 7, and 28 d post injection for the B,D) long-term experiment. The mass concentrations equate to 1.9×10^{12} particles mL^{-1} the 100 nm particles (Equation S4, Supporting Information). Data is expressed as points for individual mice and lines for the arithmetic mean (A,B), or as the average percentage fraction of the total observable fluorescence in all organs (B,D). Sample sizes were as follows for each time point 1 h ($n = 2$), 2 h ($n = 4$), 4 h ($n = 4$), 8 h ($n = 4$), or 24 h ($n = 4$) (A,C), and $n = 4$ (B,D).

Remarkably, this is only valid for nanoparticles of the size of 100 nm and above, as the difference in rigidity for particles below 50 nm is negligible. Our experiments also suggest that the differences in internalization observed can be attributed to a preference of those softer particles for non-receptor-mediated endocytotic pathways. In contrast, there is a substantial preference of the harder nanoparticles for the caveolae-mediated endocytosis, a well-known cellular mechanosensing system, indicating rigidity may affect sub-cellular processes, which will be an area of further investigation. Nevertheless, minimal differences were observed in the organ biodistribution and tumor accumulation of hard and soft 100 nm particles. Overall, our work highlights the importance of studying the interactions between multiple physio-chemical properties of nanomaterials and biological systems. We believe the information reported here will aid the design of more effective nanoparticles for biomedical purposes.

4. Experimental Section

Experimental section can be found in the Supporting Information. All animal experiments were conducted at the University of Warwick and under the approval of the local AWERB committee as well as Home Office License (70/8536).

Supporting Information

Supporting Information is available from the Wiley Online Library or from the author.

© 2022 The Authors. Small published by Wiley-VCH GmbH

Acknowledgements

P.G. and C.S.-C. contributed equally to this work. The Monash-Warwick Alliance (PG; JZ; SE; SP), CRUK/EPSRC (Grant No. C53561/A19933; SP; PG; CSC); the German Research Foundation (DFG, GZ: HA 7725/1-1; MH) and the Warwick Cancer Research Centre are acknowledged for funding. The authors would like to thank Dr Saskia Bakker for her help with Cryo-TEM analysis and acknowledge the University of Warwick Advanced BioImaging Research Technology Platform, and BBSRC ALERT14 award BB/M01228X/1 for funding. The authors also thank Bert van der Horst for supplying Hepa1-6 cells. The authors are also grateful to Dr Kai Yu and Dr Olivier Cayre (School of Chemical and Process Engineering, University of Leeds, Leeds, LS2 9JT, UK) for assistance with AFM analysis and data interpretation.

Conflict of Interest

The authors declare no conflict of interest.

Data Availability Statement

The data that support the findings of this study are available from the corresponding author upon reasonable request.

Keywords

cellular uptake, elasticity, endocytosis, glass transition temperature, in vivo distribution, nanoparticles, RAFT emulsion polymerization, rigidity

Received: May 18, 2022
Revised: July 11, 2022
Published online:

[1] T. Sun, Y. S. Zhang, B. Pang, D. C. Hyun, M. Yang, Y. Xia, *Angew. Chem., Int. Ed.* **2014**, *53*, 12320.
[2] S. K. Nune, P. Gunda, P. K. Thallapally, Y.-Y. Lin, L. M. Forrest, C. J. Berkland, *Expert Opin. Drug Delivery* **2009**, *6*, 1175.
[3] S. Parveen, R. Misra, S. K. Sahoo, *Nanomed.: Nanotechnol. Biol. Med.* **2012**, *8*, 147.
[4] A. B. Cook, P. Decuzzi, *ACS Nano* **2021**, *15*, 2068.
[5] J.-W. W. Yoo, E. Chambers, S. Mitragotri, *Curr. Pharm. Des.* **2010**, *16*, 2298.
[6] S.-D. Li, L. Huang, *J. Controlled Release* **2010**, *145*, 178.
[7] R. Gref, M. Lück, P. Quellec, M. Marchand, E. Dellacherie, S. Harnisch, T. Blunk, R. Müller, *Colloids Surf., B* **2000**, *18*, 301.
[8] P. Gurnani, S. Perrier, *Prog. Polym. Sci.* **2020**, *102*, 101209.
[9] H. Maeda, *J. Controlled Release* **2012**, *164*, 138.
[10] J. Fang, H. Nakamura, H. Maeda, *Adv. Drug Delivery Rev.* **2011**, *63*, 136.
[11] W. Wang, K. Gaus, R. D. Tilley, J. J. Gooding, *Mater. Horiz.* **2019**, *6*, 1538.
[12] X. Bai, F. Liu, Y. Liu, C. Li, S. Wang, H. Zhou, W. Wang, H. Zhu, D. A. Winkler, B. Yan, *Toxicol. Appl. Pharmacol.* **2017**, *323*, 66.
[13] X.-Q. Zhang, X. Xu, N. Bertrand, E. Pridgen, A. Swami, O. C. Farokhzad, *Adv. Drug Delivery Rev.* **2012**, *64*, 1363.
[14] N. Hoshyar, S. Gray, H. Han, G. Bao, *Nanomedicine* **2016**, *11*, 673.
[15] C. He, Y. Hu, L. Yin, C. Tang, C. Yin, *Biomaterials* **2010**, *31*, 3657.
[16] N. Ma, C. Ma, C. Li, T. Wang, Y. Tang, H. Wang, X. Mou, Z. Chen, N. He, *J. Nanosci. Nanotechnol.* **2013**, *13*, 6485.
[17] X. Huang, X. Teng, D. Chen, F. Tang, J. He, *Biomaterials* **2010**, *31*, 438.
[18] J. A. Champion, Y. K. Katare, S. Mitragotri, *J. Controlled Release* **2007**, *121*, 3.
[19] E. Fröhlich, *Int. J. Nanomed.* **2012**, *7*, 5577.
[20] Z.-G. Yue, W. Wei, P.-P. Lv, H. Yue, L.-Y. Wang, Z.-G. Su, G.-H. Ma, *Biomacromolecules* **2011**, *12*, 2440.
[21] L. Ho, W.-Y. Yung, K. Sy, H. Li, C. K. Choi, K. Leung, T. W. Y. Lee, C. Choi, *ACS Nano* **2017**, *11*, 6085.
[22] S. A. Kulkarni, S.-S. Feng, *Pharm. Res.* **2013**, *30*, 2512.
[23] Y. Hui, D. Wibowo, Y. Liu, R. Ran, H.-F. Wang, A. Seth, A. P. J. Middelberg, C.-X. Zhao, *ACS Nano* **2018**, *12*, 2846.
[24] Z. Li, C. Xiao, T. Yong, Z. Li, L. Gan, X. Yang, *Chem. Soc. Rev.* **2020**, *49*, 2273.
[25] O. Chaudhuri, S. T. Koshy, C. Cunha, J.-W. Shin, C. S. Verbeke, K. H. Allison, D. J. Mooney, *Nat. Mater.* **2014**, *13*, 970.
[26] T. Yeung, P. C. Georges, L. A. Flanagan, B. Marg, M. Ortiz, M. Funaki, N. Zahir, W. Ming, V. Weaver, P. A. Janmey, *Cell Motil. Cytoskeleton* **2005**, *60*, 24.
[27] A. J. Engler, S. Sen, H. L. Sweeney, D. E. Discher, *Cell* **2006**, *126*, 677.
[28] B. Eshaghi, N. Alsharif, X. An, H. Akiyama, K. A. Brown, S. Gummuluru, B. M. Reinhard, *Adv. Sci.* **2020**, *7*, 2000649.
[29] J. Key, A. L. Palange, F. Gentile, S. Aryal, C. Stigliano, D. Di Mascolo, E. De Rosa, M. Cho, Y. Lee, J. Singh, P. Decuzzi, *ACS Nano* **2015**, *9*, 11628.
[30] A. C. Anselmo, M. Zhang, S. Kumar, D. R. Vogus, S. Menegatti, M. E. Helgeson, S. Mitragotri, *ACS Nano* **2015**, *9*, 3169.
[31] Y. Hui, X. Yi, F. Hou, D. Wibowo, F. Zhang, D. Zhao, H. Gao, C.-X. Zhao, *ACS Nano* **2019**, *13*, 7410.
[32] H. Deng, K. Song, J. Zhang, L. Deng, A. Dong, Z. Qin, *Chem. Commun.* **2018**, *54*, 3014.
[33] P. Guo, D. Liu, K. Subramanyam, B. Wang, J. Yang, J. Huang, D. T. Auguste, M. A. Moses, *Nat. Commun.* **2018**, *9*, 130.
[34] Y. Takechi-Haraya, Y. Goda, K. Sakai-Kato, *Mol. Pharmaceutics* **2017**, *14*, 2158.
[35] L. Zhang, Q. Feng, J. Wang, S. Zhang, B. Ding, Y. Wei, M. Dong, J.-Y. Ryu, T.-Y. Yoon, X. Shi, J. Sun, X. Jiang, *ACS Nano* **2015**, *9*, 9912.
[36] Y. Hui, X. Yi, D. Wibowo, G. Yang, A. P. J. Middelberg, H. Gao, C.-X. Zhao, *Sci. Adv.* **2020**, *6*, eaaz4316.
[37] H. Sun, E. H. H. H. H. Wong, Y. Yan, J. Cui, Q. Dai, J. Guo, G. G. Qiao, F. Caruso, *Chem. Sci.* **2015**, *6*, 3505.
[38] R. Hartmann, M. Weidenbach, M. Neubauer, A. Fery, W. J. Parak, *Angew. Chem., Int. Ed.* **2015**, *54*, 1365.
[39] W. Liu, X. Zhou, Z. Mao, D. Yu, B. Wang, C. Gao, *Soft Matter* **2012**, *8*, 9235.
[40] A. C. Anselmo, S. Mitragotri, *Adv. Drug Delivery Rev.* **2017**, *108*, 51.
[41] R. Singh, J. W. Lillard, *Exp. Mol. Pathol.* **2009**, *86*, 215.
[42] Z. Shen, H. Ye, X. Yi, Y. Li, *ACS Nano* **2019**, *13*, 215.
[43] J. Sun, L. Zhang, J. Wang, Q. Feng, D. Liu, Q. Yin, D. Xu, Y. Wei, B. Ding, X. Shi, X. Jiang, *Adv. Mater.* **2015**, *27*, 1402.
[44] K. Raemdonck, J. Demeester, S. Smedt, *Soft Matter* **2008**, *5*, 707.
[45] K. S. Anseth, C. N. Bowman, L. Brannon-Peppas, *Biomaterials* **1996**, *17*, 1647.
[46] A. Johnston, C. Cortez, A. S. Angelatos, F. Caruso, *Curr. Opin. Colloid Interface Sci.* **2006**, *11*, 203.
[47] K. L. Ngai, D. J. Plazek, *Rubber Chem. Technol.* **1995**, *68*, 376.
[48] J. Zhao, H. Lu, Y. Yao, S. Ganda, M. H. Stenzel, *J. Mater. Chem. B* **2018**, *6*, 4223.
[49] S. Lorenz, C. P. Hauser, B. Autenrieth, C. K. Weiss, K. Landfester, V. Mailänder, *Macromol. Biosci.* **2010**, *10*, 1034.
[50] S. Perrier, P. Takolpuckdee, *J. Polym. Sci., Part A: Polym. Chem.* **2005**, *43*, 5347.
[51] J. Chiefari, Y. K. Chong, F. Ercole, J. Krstina, J. Jeffery, T. P. T. Le, R. T. A. Mayadunne, G. F. Meijs, C. L. Moad, G. Moad, E. Rizzardo, S. H. Thang, *Macromolecules* **1998**, *31*, 5559.

© 2022 The Authors. Small published by Wiley-VCH GmbH

[52] R. A. E. Richardson, T. R. Guimarães, M. Khan, G. Moad, P. B. Zetterlund, S. Perrier, *Macromolecules* **2020**, *53*, 7672.
[53] J. Ugelstad, F. Hansen, *Rubber Chem. Technol.* **1976**, *49*, 536.
[54] C. J. Ferguson, R. J. Hughes, D. Nguyen, B. T. Pham, R. G. Gilbert, A. K. Serelis, C. H. Such, B. S. Hawkett, *Macromolecules* **2005**, *38*, 2191.
[55] S. L. Canning, G. N. Smith, S. P. Armes, *Macromolecules* **2016**, *49*, 1985.
[56] P. Gurnani, A. M. Lunn, S. Perrier, *Polymer* **2016**, *106*, 229.
[57] P. Gurnani, A. B. Cook, R. A. E. Richardson, S. Perrier, *Polym. Chem.* **2019**, *10*, 1452.
[58] J. Lesage de la Haye, X. Zhang, I. Chaduc, F. Brunel, M. Lansalot, F. D'Agosto, *Angew. Chem., Int. Ed.* **2016**, *55*, 3739.
[59] I. Chaduc, E. Reynaud, L. Dumas, L. Albertin, F. D'Agosto, M. Lansalot, *Polymer* **2016**, *106*, 218.
[60] P. Gurnani, C. Sanchez-Cano, K. Abraham, H. Xandri-Monje, A. B. Cook, M. Hartlieb, F. Lévi, R. Dallmann, S. Perrier, *Macromol. Biosci.* **2018**, *18*, 1800213.
[61] P. Gurnani, C. P. Bray, R. A. E. Richardson, R. Peltier, S. Perrier, *Macromol. Rapid. Commun.* **2018**, *40*, 1800314.
[62] R. Hiorns, *Polym. Int.* **2000**, *49*, 807.
[63] N. P. Truong, M. V. Dussert, M. R. Whittaker, J. F. Quinn, T. P. Davis, *Polym. Chem.* **2015**, *6*, 3865.
[64] M. Chenal, L. Bouteiller, J. Rieger, *Polym. Chem.* **2013**, *4*, 752.
[65] C. Grazon, J. Rieger, R. Méallet-Renault, B. Charleux, G. Clavier, *Macromolecules* **2013**, *46*, 5167.
[66] R. L. Ball, C. M. Knapp, K. A. Whitehead, *PLoS One* **2015**, *10*, e0133154.
[67] Y. Song, R. Guan, F. Lyu, T. Kang, Y. Wu, X. Chen, *Mutat. Res.* **2014**, *769*, 113.
[68] H. J. Je, E. S. Kim, J.-S. Lee, H. G. Lee, *J. Agric. Food Chem.* **2017**, *65*, 10899.
[69] W. He, M. J. Bennett, L. Luistro, D. Carvajal, T. Nevins, M. Smith, G. Tyagi, J. Cai, X. Wei, T.-A. Lin, D. C. Heimbrook, K. Packman, J. F. Boylan, *Mol. Ther.* **2014**, *22*, 359.
[70] E. Rivero-Buceta, C. Vidaurre-Agut, C. D. Vera-Donoso, J. M. Benlloch, V. Moreno-Manzano, P. Botella, *ACS Omega* **2019**, *4*, 1281.
[71] L. Martin, R. Peltier, A. Kuroki, J. S. Town, S. Perrier, *Biomacromolecules* **2018**, *19*, 3190.
[72] N. G. Lamson, A. Berger, K. C. Fein, K. A. Whitehead, *Nat. Biomed. Eng.* **2020**, *4*, 84.
[73] C. Cortés, J. Domenech, M. Salazar, S. Pastor, R. Marcos, A. Hernández, *Environ. Sci.: Nano* **2020**, *7*, 272.
[74] I. D. Angelis, L. Turco, *Curr. Protoc. Toxicol.* **2011**, *47*, 20.6.1.
[75] J. M. Torres, C. M. Stafford, B. D. Vogt, *ACS Nano* **2009**, *3*, 2677.
[76] G. J. Doherty, H. T. McMahon, *Annu. Rev. Biochem.* **2009**, *78*, 857.
[77] J. J. Rennick, A. P. R. Johnston, R. G. Parton, *Nat. Nanotech.* **2021**, *16*, 266.
[78] S. Zhang, H. Gao, G. Bao, *ACS Nano* **2015**, *9*, 8655.
[79] Z. Mao, X. Zhou, C. Gao, *Biomater. Sci.* **2013**, *1*, 896.
[80] C. Dombu, M. Kroubi, R. Zibouche, R. Matran, D. Betbeder, *Nanotechnology* **2010**, *21*, 355102.
[81] R. G. Parton, M. A. del Pozo, *Nat. Rev. Mol. Cell Biol.* **2013**, *14*, 98.
[82] E. Spisni, M. C. Bianco, C. Griffoni, M. Toni, R. D'Angelo, S. Santi, M. Riccio, V. Tomasi, *J. Cell. Physiol.* **2003**, *197*, 198.
[83] L. De Smet, W. Ceelen, J. P. Remon, C. Vervaet, *Sci. World. J.* **2013**, *2013*, 7.
[84] A. Garapaty, J. A. Champion, *Bioeng. Transl. Med.* **2017**, *2*, 92.
[85] F. Alexis, E. Pridgen, L. K. Molnar, O. C. Farokhzad, *Mol. Pharmaceutics* **2008**, *5*, 505.

© 2022 The Authors. Small published by Wiley-VCH GmbH